Multifunctionality of Crystalline MoV(TeNb) M1 Oxide Catalysts in Selective Oxidation of Propane and Benzyl Alcohol

Kazuhiko Amakawa,[†] Yury V. Kolen'ko,[†,‡] Alberto Villa,[§] Manfred E/ Schuster,[†] Lénárd-István Csepei,[†] Gisela Weinberg,[†] Sabine Wrabetz,[†] Raoul Naumann d'Alnoncourt,[†] Frank Girgsdies,[†] Laura Prati,[§] Robert Schlögl,[†] and Annette Trunschke*,[†]

[†]Department of Inorganic Chemistry, Fritz-Haber-Institute der Max-Planck-Gesellschaft, Faradayweg 4-6, 14195 Berlin, Germany
[§]Department of Inorganic Chemistry, University of Milan, Via Venezian 21, I-20133 Milan, Italy

Ⓢ Supporting Information

ABSTRACT: Propane oxidation at 653−673 K and benzyl alcohol oxidation at 393 K over phase-pure MoV(TeNb) M1 oxide catalysts were studied to gain insight into the multiple catalytic functions of the surface of the M1 structure. Electron microscopy and X-ray diffraction confirmed the phase purity of the M1 catalysts. Propane oxidation yields acrylic acid via propene as intermediate, while benzyl alcohol oxidation gives benzaldehyde, benzoic acid, benzyl benzoate, and toluene. The

consumption rates of benzyl alcohol and propane level in the same range despite huge difference in reaction temperature, suggesting high activity of M1 for alcohol oxidation. Metal−oxygen sites on the M1 surface are responsible for the conversion of the two reactants. However, different types of active sites and reaction mechanisms may be involved. Omitting Te and Nb from the M1 framework eliminates acrylic acid selectivity in propane oxidation, while the product distribution in benzyl alcohol oxidation remains unchanged. The results suggest that the surface of M1 possesses several types of active sites that likely perform a complex interplay under the harsh propane oxidation condition. Possible reaction pathways and mechanisms are discussed.

KEYWORDS: propane, benzyl alcohol, selective oxidation, acrylic acid, M1, mixed oxide, MoVTeNbO, multifunctionality
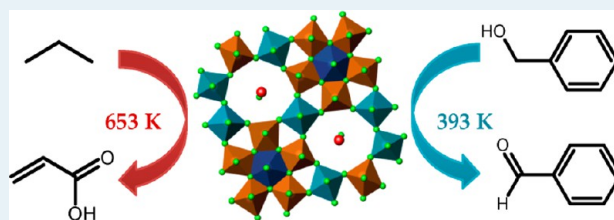
1. INTRODUCTION

Chemical utilization of light alkanes in natural gas and refinery off-gases is an important research area in the context of sustainability, in which selective partial oxidation represents a major issue. Crystalline MoVTeNb oxides developed by Mitsubishi Chemicals[1] are among the best performing catalysts in propane oxidation and ammoxidation to acrylic acid and acrylonitrile at 613−693 K.[2,3]

The direct conversion of propane to acrylic acid involves abstraction of four hydrogen atoms, addition of two oxygen atoms and transfer of eight electrons. Both hydrogen abstraction and oxygen addition are oxidation reactions, however, require substantially different quality of active oxygen species.[4] Hence, successful catalysts should be equipped with multiple oxidation functionalities. A proper interplay of catalytic functions is necessary to accomplish pathways to selective oxidation products while avoiding the overoxidation to CO_x.

It has been established that the orthorhombic M1 phase (ICSD no. 55097)[5] alone is able to accomplish transformation of propane to acrylic acid.[2,6−11] The crystal structure of quinary M1 consists of corner-sharing MO_6 (M = Mo, V) octahedra forming a layer in the (001) plane. This layer has hepta-, hexa-, and pentagonal voids. The latter ones are occupied by NbO_7 pentagonal bipyramids, while TeO units partially occupy the hexa- and heptagonal voids (Scheme 1). Such layers are stacked via metal−oxygen bonds along the (001) direction sharing

corners of the polyhedra and forming elongated M1 particles. The M1 structure allows certain flexibility with respect to the occupancy of metal framework positions. The formation of ternary MoV M1 oxide is possible. It is assumed that the hexa- and heptagonal voids of the resulting M1 are unoccupied in this case. The ternary MoV M1 oxide can activate propane but leads to nonselective oxidation to carbon oxides.[12,13]

Highly performing and well-defined bulk catalysts composed of the M1 structure[14−16] provide a suitable opportunity to address structure−function relationships in complex oxidation reaction. Based on the site isolation concept and considering classic organic chemistry as well as the crystal structure of M1,[17] Grasselli and co-workers proposed that propane can be converted to acrylic acid over specific sites existing in the basal (001) plane of the M1 structure without desorption of intermediates.[18] The attempts to experimentally examine the effectiveness of the (001) plane have resulted in contradictive conclusions.[19,20] Experimental evidence for the deviation of the surface chemical composition from the bulk has inspired functional models of monolayer-type active sites "supported" on the bulk M1 structure.[7,13,21−23] Recently, we found dynamic changes in the chemical composition of the M1 surface under

Scheme 1. Unit Cell of M1 Projected along [001][a]
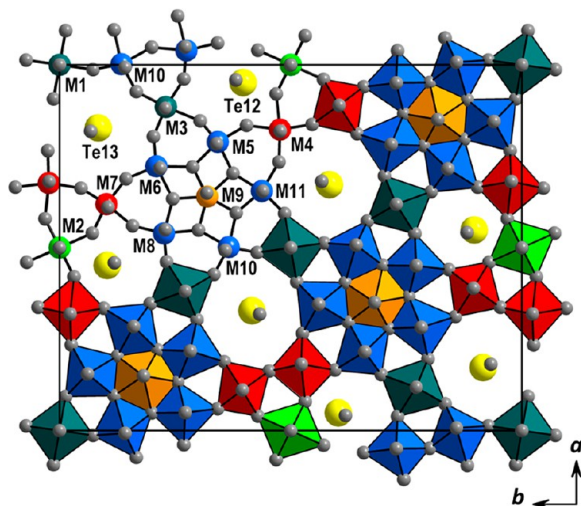
[a]One asymmetric unit is shown in ball-and-stick representation, with numbering of non-O atom sites following DeSanto et al.[5] Different colors for mixed metal sites M = (Mo, V, Nb) are chosen to reflect their different topologies not the distribution of elements.

reaction conditions, which correlate with the evolution of acrylic acid formation.[23] Irrespective of the specific active site model, it is generally assumed that V is the key element for the propane activation, while the presence of Nb and particularly Te seem to be related to the selectivity to acrylic acid.[7,12,13,21,23]

The reaction network and underlying catalytic functions of MoVTeNb M1 oxide have been addressed by kinetic investigations, as well as reactivity studies of potential intermediates.[7,11,12,24−28] Propene is a major intermediate, which undergoes further oxygenation to acrylic acid. The oxidative dehydrogenation of propane (ODP) to propene is a slow step, while consecutive oxidation of propene to acrylic acid is a kinetically much faster reaction. Besides propene, other C3 intermediates are seldom detected. The M1 phase efficiently transforms potential intermediates in the acrylic acid formation (i.e., propene, allyl alcohol, and acrolein) at reaction temperature lower than that of propane.[7,11,12,28] The ternary MoV M1 oxide serves as excellent catalyst for acrolein oxidation to acrylic acid at temperature as low as 463 K.[29]

Interestingly, the M1 phase shows versatile performance in selective oxidation of reactants beyond alkanes. Besides above-mentioned propene, allyl alcohol, and acrolein, oxidation of alcohols at low temperature has been explored. MoVTeNb mixed oxides catalyze gas-phase ethanol oxidation to acetic acid above 473 K.[30] Ternary MoV M1 oxide is active in liquid-phase benzyl alcohol oxidation to benzaldehyde at 353 K.[31−33] Considering the dynamics of the M1 surface,[22,23] the state of the M1 surface under conditions of liquid-phase reactions may deviate from that under propane oxidation condition. Nevertheless, we consider that the low temperature oxidation catalysis could indicate also some catalytic functions possibly involved in propane oxidation. Alcohol and aldehyde intermediates (either in the gas-phase or on the surface) are likely involved in the acrylic acid formation,[2] although these are seldom detected in the gas-phase likely because of rapid consecutive reactions that lead to stable end products (e.g., acrylic acid, CO, and CO_2). Studying alcohol oxidation at low temperature may bring information on catalytic functions

working but invisible in propane oxidation, allowing deeper understanding of the multifunctionality of M1.

In this paper, we describe a comparative study of gas-phase propane oxidation at 653−673 K and liquid-phase benzyl alcohol oxidation at 393 K. Carefully prepared and characterized phase-pure quinary MoVTeNb oxide and ternary MoV oxide catalysts composed of the orthorhombic M1 structure are used to investigate the role of the constituent elements of the M1 phase. The comparative reactivity study sheds light on catalytic function of the M1 phase in an extend range of reaction condition.

2. EXPERIMENTAL SECTION

2.1. Preparation of the Catalysts. *2.1.1. Catalysts I-a and I-b.* Nanocrystalline quinary MoVTeNb M1 oxide catalysts were synthesized following a protocol developed in our laboratory.[27] Briefly, 0.08 mol of molybdenum(VI) oxide (MoO₃; Fluka 99.5%) and 0.1 mol of oxalic acid dihydrate ($C_2H_2O_4 \cdot 2H_2O$; ROTH 99.5%) were dissolved in 0.2 L of water (Milli-Q Synthesis System) at 353 K. The solution was allowed to cool to 338 K and then an appropriate amount of telluric acid ($Te(OH)_6$; Aldrich 97.5−102.5%) was dissolved. In parallel, the V-containing solution was prepared by dissolution of vanadium(V) oxide (V_2O_5; Riedel-de Haën 99.5%) together with $C_2H_2O_4 \cdot 2H_2O$ (50% excess by mol) in 0.1 L of water at 338 K. Next, this solution was added to the Mo/Te-containing one, the solution was allowed to cool to 313 K, and then an appropriate amount of ammonium niobate(V) oxalate hydrate ($NH_4[NbO(C_2O_4)_2] \cdot xH_2O$, 20.2% of Nb; H. C. Starck 99.99%) was dissolved. In this way, the Mo/V/Te/Nb-containing oxalic complex solutions with nominal molar ratios Mo:V:Te:Nb of 1:0.26:0.15:0.13 (**I-a**) or 1:0.225:0.15:0.1535 (**I-b**) were prepared. To obtain a powder from the solutions, spray-drying was performed (Büchi B-191 mini spray-dryer). The resultant product was calcined (548 K, 1 h, air flow) using a rotary tube furnace (Xerion), and then subjected to the superheated-water vapor treatment (SWVT). Repeatedly, 3 g of the precursor and 2.7 g of water were charged into a 48 mL stainless steel vessel, the vessel was capped and placed inside a bomb. The bomb was sealed and kept at 773 K for 2 h under autogenous pressure of ∼20 MPa. The spatula-collected product of the SWVT was washed with water, dried, and finally annealed (873 K, 2 h, Ar flow 100 mL/min) using a rotary tube furnace (catalyst **I-a**, internal ID 6722; **I-b**, internal ID 5737).

2.1.2. Catalyst II. Synthesis of submicrocrystalline quinary MoVTeNb oxide M1 was accomplished by spray-drying and subsequent purification.[27] In short, 0.0929 mol of ammonium heptamolybdate(VI) tetrahydrate (($NH_4)_6Mo_7O_{24} \cdot 4H_2O$; Merck, GR for analysis) was dissolved in 1.5 L of water at 353 K and subsequently 0.195 mol of ammonium (meta)-vanadate(V) (NH_4VO_3; Fluka 99.0%) was dissolved therein. The solution was allowed to cool to 313 K, and then 0.1495 mol of $Te(OH)_6$ was added. In parallel, the Nb-containing solution was prepared by dissolution of 0.0813 mol of $NH_4[NbO(C_2O_4)_2] \cdot xH_2O$ in 0.5 L of water at 313 K. This solution was added to the Mo/V/Te-containing one, and then the total volume was completed to 2.5 L with water. The resultant slurry with nominal molar ratio Mo/V/Te/Nb of 1:0.3:0.23:0.125 was first spray-dried and the product was then calcined (548 K, 1 h, air flow 100 mL/min) and finally annealed (873 K, 2 h, Ar flow) using a rotary tube furnace. As a result, the powder containing crystalline M1 and M2 phases was

Table 1. Compositional and Textural Details of the Synthesized Phase-Pure M1-Type Oxides

catalyst	chemical composition[a]	surface composition[b]	surface area[c] ($m^2 g^{-1}$)	pore volume[d] ($cm^3 g^{-1}$)
I-a	$Mo_1V_{0.26}Te_{0.08}Nb_{0.13}O_x$	n.d.	15.7	0.003
I-b	$Mo_1V_{0.23}Te_{0.09}Nb_{0.24}O_x$	$Mo_1V_{0.10}Te_{0.08}Nb_{0.22}$	13.3	0.002
II	$Mo_1V_{0.26}Te_{0.11}Nb_{0.22}O_x$	$Mo_1V_{0.30}Te_{0.50}Nb_{0.11}$	7.5	0.012
III	$Mo_1V_{0.37}O_x$	n.d.	35.7	0.010

[a]EDX data (all values are the average of at least five probed areas). [b]XPS data measured in presence of 0.25 mbar O_2 at 298 K including information from a depth of approximately 3 nm [c]Calculated from nitrogen by using the BET method. [d]Calculated from nitrogen physisorption uptake at $p/p_0 = 0.95$ assuming cylindrical pores.

generated. Further, M1 was isolated from M2 by washing with 15% hydrogen peroxide solution (H_2O_2; Merck, GR for analysis) through stirring at 400 rpm for 24 h (solid to liquid ratio was 0.04 g/mL). The washed product was collected by vacuum filtration, washed by water, dried, and finally annealed (873 K, 2 h, Ar flow 100 mL/min) using a rotary tube furnace (catalyst **II**, internal ID 6902).

2.1.3. Catalyst III. Nanocrystalline ternary MoV M1 oxide catalyst was synthesized by a hydrothermal approach.[29] First, 0.0095 mol of $(NH_4)_6Mo_7O_{24}·4H_2O$ and 0.0159 mol of vanadium(IV) oxide sulfate pentahydrate ($VOSO_4·5H_2O$; Riedel−de Haën 95.0%) were charged into a 0.4 L Hastelloy autoclave reactor (Premex AG) backfilled with 0.26 L of water. The autoclave was sealed, and the precursor system with nominal molar ratio Mo/V of 1:0.24 was subsequently in situ homogenized (300 rpm, 343 K, 30 min). Then, the autoclave was heated to 423 K and kept at this temperature for 100 h under constant stirring of 300 rpm and autogenous pressure of ∼0.9 MPa. After it was cooled, the product was collected by centrifugation (4000 rpm, 1 h), washed with water, dried, and annealed (673 K, 2 h, Ar flow 100 mL/min) using a rotary tube furnace (catalyst **III**, internal ID 8103).

2.2. Characterization Methods. The products were characterized by powder X-ray diffraction (XRD, Bruker D8 Advanced diffractometer) analyzing the phase composition by whole pattern Rietveld fitting using the program TOPAS (Bruker AXS). The specific surface area was calculated applying the BET analysis based on N_2 physisorption measurements at 77 K (Quantachrome Autosorb-6B analyzer). Total pore volumes were estimated from the nitrogen uptake at $p/p_0 = 0.95$. Microstructure and bulk chemical composition were analyzed by scanning electron microscopy (SEM, Hitachi S-4800 microscope, operated at 3 kV), energy-dispersive X-ray spectroscopy (EDX, EDAX Genesis spectrometer attached to the SEM, operated at 15 kV), and transmission electron microscopy (TEM, Philips CM200-FEG microscope, operated at 200 kV). The surface properties of the catalysts were studied by microcalorimetry (SETARAM MS70 Calvet Calorimeter connected to a vacuum and gas dosing line), and X-ray photoelectron spectroscopy using the monochromatic radiation of the ISISS (Innovative Station for in situ Spectroscopy) beamline of the synchrotron radiation facility BESSY II (Helmholtz-Zentrum, Berlin).

2.3. Gas-Phase Propane Oxidation. The gas-phase propane oxidation was carried out in a fixed-bed tubular reactor in continuous flow mode. Typically, 1 g of powdered catalyst was first binder-free pressed under ∼185 MPa, crushed and sieved to a particle size of 250−355 μm. Then, 300 mg of the catalyst diluted with 1 g of silicon carbide (both 250−355 μm sized) were loaded into a tubular reactor. The feed was composed of C_3H_8, O_2, H_2O, and N_2 in a molar ratio of 3:6:40:51 vol.-%. The reaction was carried out at 653 or 673 K

and atmospheric pressure while total flow rate was varied to acquire propane conversion in a range between 5 and 50%. Inlet and outlet gases were analyzed by online gas chromatography (GC) using a GC system (Agilent Technologies 7890A or 6890N). A Plot molecular sieve column and a PlotQ column were used for the analysis of O_2, N_2, CO, and CO_2. Hydrocarbons and oxygenates were monitored employing a HP-FFAP capillary column and a PlotQ column. The conversion of propane and selectivity were calculated based on the total number of carbon atoms and the products found. The conversion of dioxygen was calculated based on the concentration difference between inlet and outlet.

2.4. Liquid-Phase Benzyl Alcohol Oxidation. The liquid-phase benzyl alcohol oxidation was carried out in a temperature-controlled glass reactor (30 mL) in conjunction with a reservoir (5 L) containing oxygen at 2 atm. The oxidation experiments were carried out solventless (typically, 10 g of benzyl alcohol (purity was confirmed by gas chromatography), 0.5 g of the catalyst, $T = 120$ °C, $P_{O_2} = 2$ atm) employing controlled magnetic stirring. Periodic removal of samples from the reactor was performed and the reaction products were identified and analyzed by GC and GC coupled with mass spectrometry (GC-MS) using a Dani 86.10 HT gas chromatograph. A BP21 capillary column (length 30 m, inner diameter 0.53 mm, film thickness 0.5 μm) from SGE Analytical Science was used. For quantification of reactants and products, the external calibration method was applied. The oxygen uptake was followed by a mass-flow controller connected to a PC using an A/D board.

3. RESULTS AND DISCUSSION

3.1. Structural Characterization of Phase-Pure M1. Elemental composition, surface composition, surface area, and total pore volume of the synthesized catalysts are summarized in Table 1. Nitrogen adsorption isotherms (now shown) of all the catalysts show the features of macroporous materials, reflected in relatively low specific surface areas, and pore volumes (Table 1).

Rietveld analysis (Supporting Information Figures S1−S4) of the XRD patterns (Figure 1) confirms that all the catalysts **I-a**, **I-b**, **II**, and **III** consist of single-phase orthorhombic M1-type structure (ICSD no. 55097). The XRD pattern of catalyst **III** shows strong anisotropic peak broadening because of preferential crystallization along the c direction, which is in accordance with thin needle-like morphology, as revealed by the SEM and TEM observations (Figures 2 and 3).

The representative SEM images are displayed in Figure 2. The quinary MoVTeNb M1 oxide **I-a**, **I-b**, and **II** show moderate aggregated powders composed of two types of particles: submicrometer-sized faceted rods having a prismatic crystallinity, and smaller, nearly rectangular particles. The particle size of the smaller particles in **II** is bigger than in **I-a**
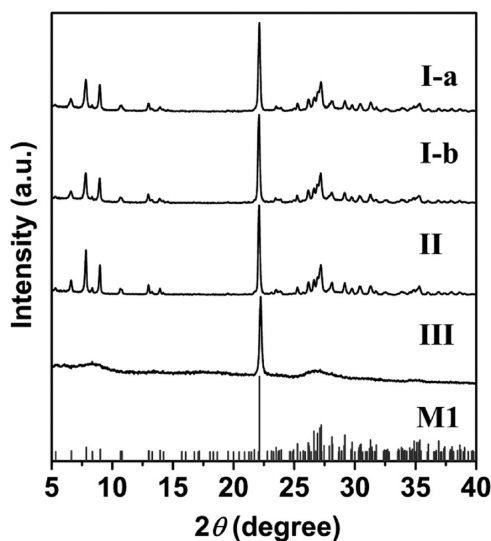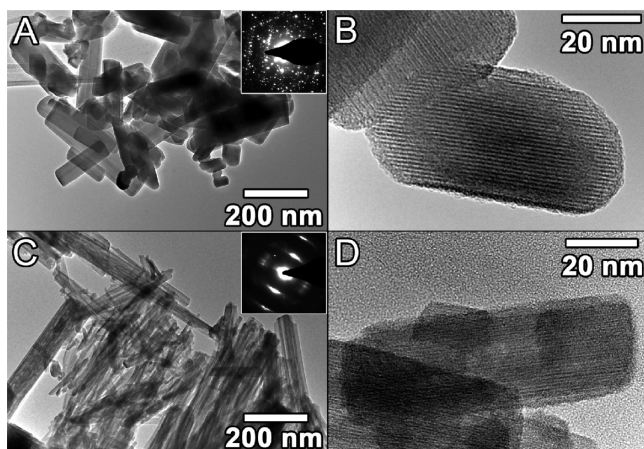
Figure 1. Powder X-ray diffraction patterns of the synthesized catalysts. Tick marks below the patterns correspond to the positions of the Bragg reflections expected for the orthorhombic M1 phase (ICSD no. 55097).
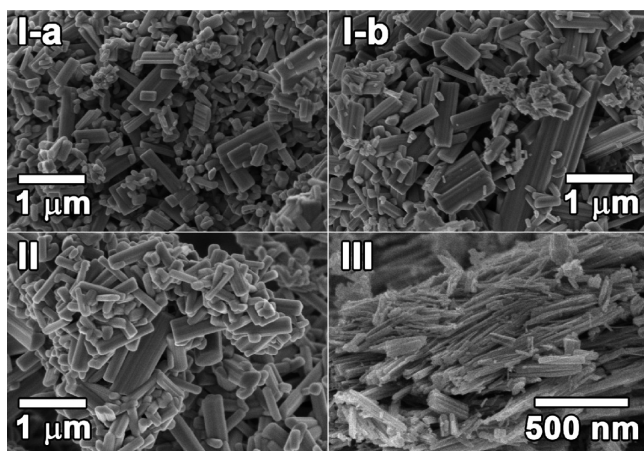
**Figure 2.** Representative SEM images of the synthesized catalysts.

Figure 3. Representative low-magnification and high-resolution TEM images of the catalysts **I-a** (A and B) and **III** (C and D). The insets in panels C and D are the respective electron diffraction patterns.

and **I-b**, which agrees with the smaller specific surface area of the catalyst **II** (Table 1). In contrast, the ternary MoV oxide M1 **III** consists of arranged aggregates of very thin needles that lead to the highest surface area among all the catalysts (Table 1), indicating preferential crystal growth along the crystallographic *c* axis and suppressed growth along the *a* and *b* axes. The absence of ill-shaped particles proves the absence of amorphous phase and overall phase-purity. Homogeneity of elemental distribution was confirmed for all the catalysts by probing elemental compositions of several local areas using EDX.

The microstructure was investigated using TEM. We have previously reported that catalysts **I-b** and **II** consist of phase-pure M1.[27] Figure 3A shows a typical low-magnification TEM image of quinary MoVTeNb oxide M1 **I-a**. The powder consists of rod-like nanoparticles with different size, in good agreement with the SEM data. Electron diffraction (ED) reveals a high crystallinity of the nanocrystals, which exhibit (001) prominent growth directions, consistent with XRD. TEM analysis of the ternary M1MoV oxide **III** shows the presence of two types of nanostructures in the sample, long and short needle-like appearances (Figure 3C). According to electron diffraction, these nanoneedles can be described as crystals with M1-like structure exclusively oriented with their long axis along (001), indicating a *c*-axis growth that is consistent with the strong texturing effect observed by XRD (Figure 1). The high-resolution TEM (HRTEM) images of the catalysts **I-a** and **III** are presented in Figure 3B and 3D. In these images, single quinary and ternary oxide nanoparticles of good crystallinity with well-developed lattice fringes are seen. The **I-a** and **I-b** catalysts that were prepared by the same method with a slight difference in the starting elemental composition show very similar microstructure and textural properties (Table 1). In summary, we have synthesized nanosized (**I-a** and **I-b**) and submicrometer-sized (**II**) quinary phase-pure MoVTeNb M1 oxide as well as a nanosized phase-pure MoV M1 oxide (**III**). The characterization confirmed entire phase purity of the samples.

3.2. Gas-Phase Propane Oxidation. Catalytic performance in the gas-phase propane oxidation at 653 or 673 K was investigated by changing the contact time (Figure 4). No significant modification is detected by XRD measurements of the MoVTeNb M1 oxide (**I-b**, **II**) (not shown) and MoV oxide M1 **III** (Figure S5 in the Supporting Information) after propane oxidation, which is in line with the highly stable catalytic performance of M1.[26] Figure 4A presents the conversion of propane as a function of contact time, while the selectivity to propene, acrylic acid, and overoxidation products (i.e., sum of acetic acid and CO_x) are reported in Figures 4B−4D as a function of propane conversion. To evaluate the intrinsic activity per unit surface area, we summarize the areal activities (i.e., reaction rates normalized by the specific surface area) in Figure 5A.

3.2.1. Comparison of MoV and MoVTeNb M1 Oxidex. Both ternary MoV and quinary MoVTeNb oxides convert propane (Figure 4A). The oxidative dehydrogenation of propane (ODP) is the first reaction occurring on all the catalysts, as indicated by high propene selectivity at low propane conversion (Figure 4B). In agreement with previous reports,[7,12,34] ternary and quinary M1 oxides show a remarkable difference in the selectivity. The quinary MoVTeNb M1 oxide (**I-b** and **II**) shows high selectivity to acrylic acid with a maximum at intermediate conversion (Figure 4C). The ternary MoV M1
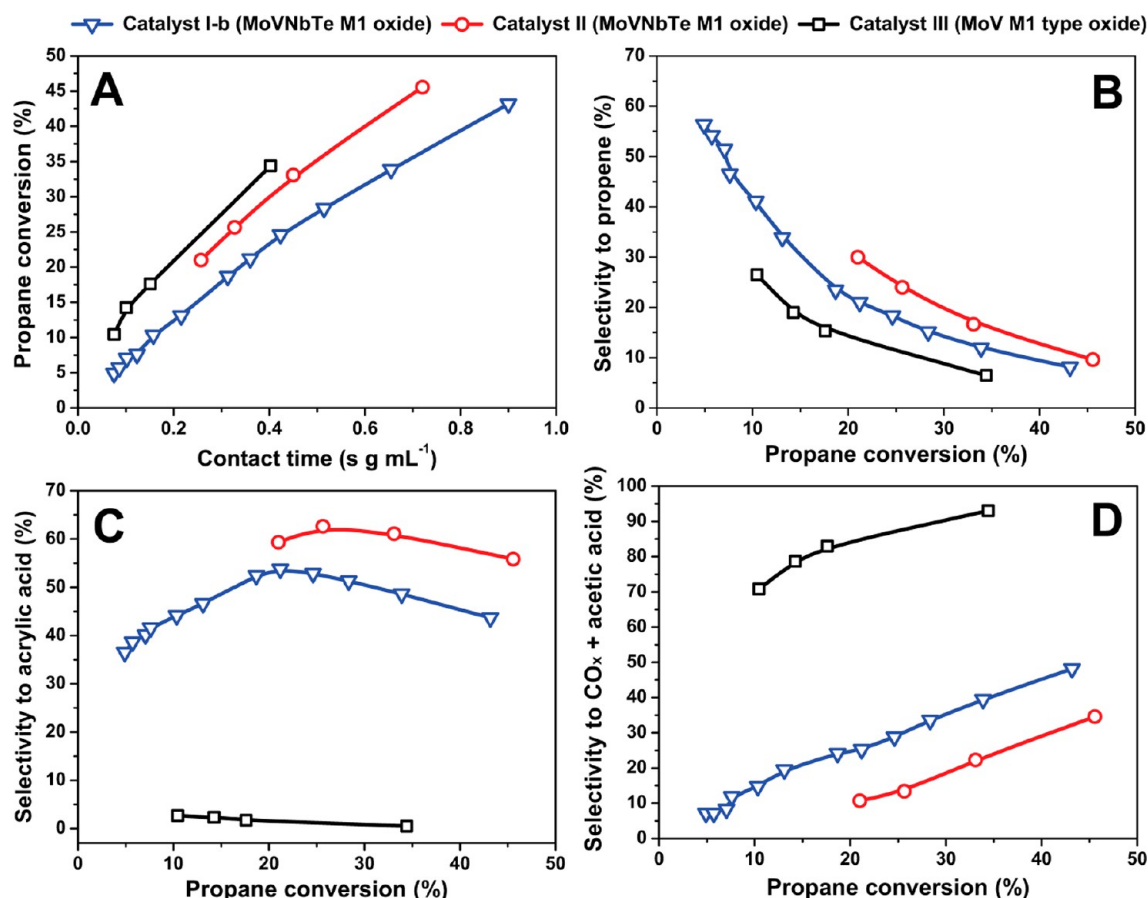
Figure 4. Catalytic performance in propane oxidation: conversion of propane versus contact time (A), as well as selectivity to propylene (B), acrylic acid (C) and acetic acid plus CO_x (D) versus conversion of propane plots. Reaction was carried out at 653 K (catalyst **I-b** and **II**) or 673 K (catalyst **III**) and a molar ratio of the feed gases $C_3H_8:O_2:H_2O:N_2$ being 3:6:40:51 vol.-%.

oxide (**III**) has the ability to activate propane to yield propene; however, it shows almost no selectivity to acrylic acid (Figure 4C) and leads to the deeper oxidation products formed by C−C bond cleavage (Figure 4D).

3.2.2. Propane Activation Step. Significant differences in the intrinsic activity of the catalysts for propane activation are observed (Figure 5A), indicating differences in the density or nature of propane activating sites. Within the quinary MoVTeNb M1 oxide catalysts, **II** shows higher intrinsic activity (Figure 5A) as well as higher selectivity to acrylic acid than **I-b** (Figure 4C). As we have previously reported,[22] the activity depends on the synthesis method even within phase-pure quinary MoVTeNb M1 oxide, leading to different surface composition (Table 1), and to different specific activity per unit surface area, most likely in consequence of variations in the surface termination. Vanadyl groups (V^{5+}=O) have been suggested to be active sites in ODP over silica-supported vanadium oxide catalysts.[35] The active sites for C−H activation in propane over polycrystalline catalysts composed of the M1-type structure are unknown but likely do not contain Te and Nb, since MoV M1 oxide **III** can also convert propane to propene. The observed lower intrinsic activity of the ternary MoV M1 oxide **III** (Figure 5A) suggests that Nb and Te may enhance the formation of the active sites by modifying the dynamic development of the active monolayer on the surface of the catalyst under reaction conditions. Adsorption of propane studied by microcalorimetry shows a weaker interaction of propane with the surface and a significantly reduced density of

propane adsorption sites on activated MoV oxide compared to activated MoVTeNb oxide.[23] The differential heats of propane adsorption as a function of the amount of adsorbed propane per unit surface area on the surface of the catalysts **I-b**, **II**, and **III** are compared in Figure 6. The comparatively high initial heats of propane adsorption on the Te-containing catalysts **I-b** and **II** of 60−65 $kJ \cdot mol^{-1}$ are consistent with our previous observations,[23] and are tentatively attributed to Te-containing adsorption sites. The abundance of these sites is higher on catalyst **II**, which is in agreement with the enhanced concentration of Te on the surface of this catalyst (Table 1). In contrast, the surface of catalyst **I-b** is depleted in Te and, consequently, only a small number of sites are found that adsorb propane more strongly. In general, the surface of **I-b** is energetically more heterogeneous compared to **II**. Strong adsorption of propane is not observed on catalyst **III**. Even though the active surface of M1 is dynamically formed under reaction conditions of propane oxidation at high temperature,[23] differences in the density of sites (Figure 5A) are reflected already in the heat of adsorption of propane measured at low temperature (Figure 6). This is probably because always the same shift in surface composition is observed on different M1 catalysts by going in the feed of the reactants from low temperature to reaction temperature, namely an enrichment of the surface in Te and V and a depletion in Mo.[22,23] Therefore, a high number of strong and energetically similar adsorption sites observed by microcalorimetry at 313 K seems to be a fingerprint for high activity in gas-phase oxidation of propane
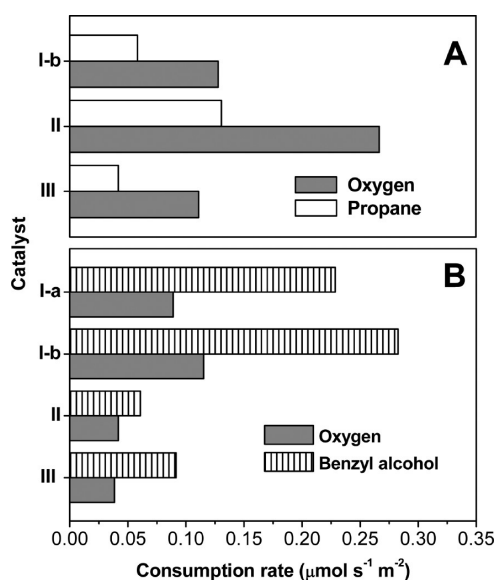
Figure 5. Surface-area-normalized consumption rates in the oxidation of propane (A) and benzyl alcohol (B). Reaction conditions of propane oxidation: T = 653 K (catalyst **I-b** and **II**) or T = 673 K (catalyst **III**), feed composition of $C_3H_8/O_2/H_2O/N_2$ = 3:6:40:51 vol.-%, contact time of 0.40–0.45 s g mL^{-1}. Reaction conditions of benzyl alcohol oxidation: T = 393 K, 10 g of benzyl alcohol, solventless, 0.5 g of catalyst, p_{O2} = 2 atm, cumulative consumption rates at reaction time of 8 h. For the data on benzyl alcohol oxidation, the consumption rates in the blank experiment ("none" in Figure 7) have been subtracted before normalizing with surface area.
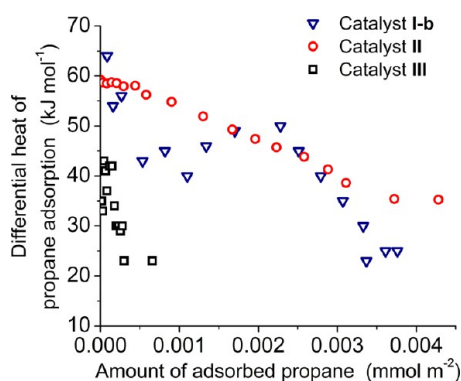
Figure 6. Differential heat of adsorption measured in the adsorption of propane as a function of surface coverage on the catalysts **I-b**, **II**, and **III** at 313 K.

at 673 K. The response of the surface composition of a ternary MoV M1 oxide catalyst toward changes in the reaction conditions is the subject of an ongoing in situ photoelectron spectroscopic study. Preliminary results indicate a more distinct enrichment of V^{5+} on the surface of MoV oxide compared to MoVTeNb oxide suggesting that not the number, but the nature of active sites is influenced by the presence of Te and Nb. The corroboration of such a hypothesis requires, however, further in situ studies by complementary methods, like Raman and IR spectroscopies.

3.2.3. Oxygen Insertion and Acrylic Acid Formation. Propene is detected in high selectivity at low propane conversion (Figure 4B). It has been proposed that propene is the predominant primary product (>95% of selectivity at the zero conversion limit) in propene oxidation over phase-pure

MoVTeNb M1 oxide.[26,27,36] It is noted that formed propene is actually released to the gas phase and travels through the catalyst bed (which is at least in millimeter scale in our reactors) before undergoing consecutive oxidation. This observation suggests two thoughts: (1) the ODP and subsequent oxidation of propene may occur at different active sites,[25] and thus, (2) copresence of the ODP sites and the sites for the propene oxidation to acrylic acid in an atomic vicinity[37] is not necessary. These thoughts are consistent with the phase cooperation effect observed in the physical mixtures of M1 and M2 phases.[18] It is also noted that the macroscopic distance between sites would also affect the reaction network, as the impact of the phase cooperation effect depends on the dimension of the phase mixing in which an intimate mixing at a micrometer scale is required to observe the synergetic effect.[18] Regarding the active sites for the selective oxidation step of propene to acrylic acid, we suggest that the ensemble sites containing V^{5+} and Te^{4+} on the topmost surface of the M1, which are dynamically formed under steam-rich propane oxidation conditions, can be responsible. In our recent ambient pressure in situ photoelectron spectroscopy study of a phase-pure MoVTeNb M1 oxide measured under propane oxidation reaction conditions, we found the depletion of Mo on the topmost surface (information depth of XPS was 0.6 nm) and the increase in the V^{5+}/V^{4+} ratio, which coincided with the increase of the acrylic acid formation upon switching the feed from dry (0 vol.-%) to steam-rich (40 vol.-%) conditions.[23] The addition of steam increases the selectivity to acrylic acid at the expense of CO_x.[23] Considering the negligible contribution of the direct combustion of propane, the selectivity in the propene oxidation step as well as the suppression of the overoxidation of acrylic acid are important issues to achieve a high selectivity to acrylic acid. Ueda and co-workers found that the presence of Te and Nb strongly suppress oxidative decomposition of acrolein and acrylic acid.[12] We consider that the formation of surface ensemble sites containing V^{5+} and Te^{4+} involves the blocking of the surface sites consisting of Mo–O–V that are responsible for CO_x formation (Figure 4D). In this way, the generation of selective oxidation sites and the elimination of unselective sites are simultaneously achieved.

3.3. Liquid-Phase Benzyl Alcohol Oxidation. Figure 7 shows the conversion of benzyl alcohol (A) and the product distribution (B) in benzyl alcohol oxidation. Figure 8 shows the evolution of the reaction over **I-a** (A) and **III** (B) along the reaction time. Figure 5B displays the consumption rates of benzyl alcohol and oxygen normalized by the surface area. To evaluate net consumption rates by heterogeneous catalysis, the consumption rates in the blank experiment (i.e., in the absence of a catalyst; "none" in Figure 7) have been subtracted before normalizing with surface area.

All the M1 catalysts can activate molecular oxygen and convert benzyl alcohol to benzaldehyde at 393 K (Figure 7). It is noted that a MoVNb oxide with Mo_5O_{14}-type structure (ICSD no. 27202), which is structurally closely related to the M1 phase, showed no additional conversion to the blank run (not shown), suggesting the importance of the M1 structure. The reaction does not proceed substantially when the system lacks either a catalyst or molecular oxygen (Figure 7), indicating heterogeneous catalysis. Possible contribution of homogeneous catalysis by leached species is excluded, because the conversion of benzyl alcohol stopped when the catalyst was filtered out at the benzyl alcohol conversion of nearly 30%. It is also noted that no hydrogen peroxide was detected in the
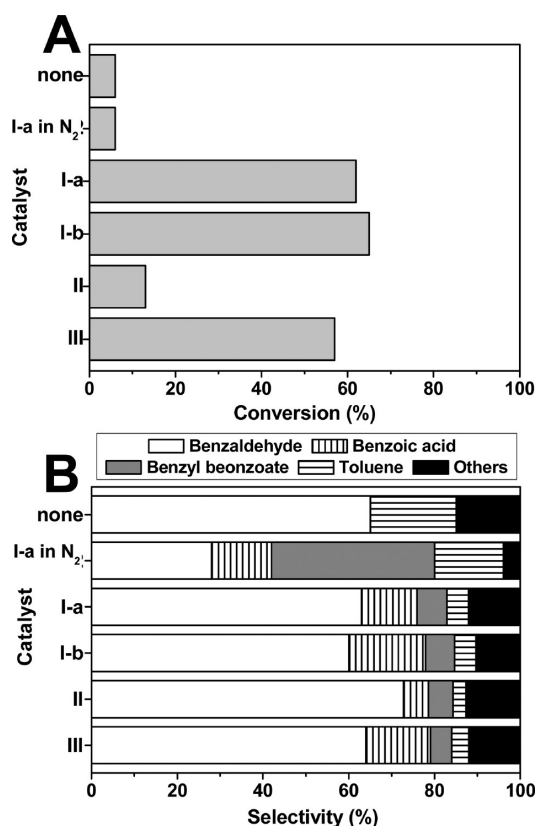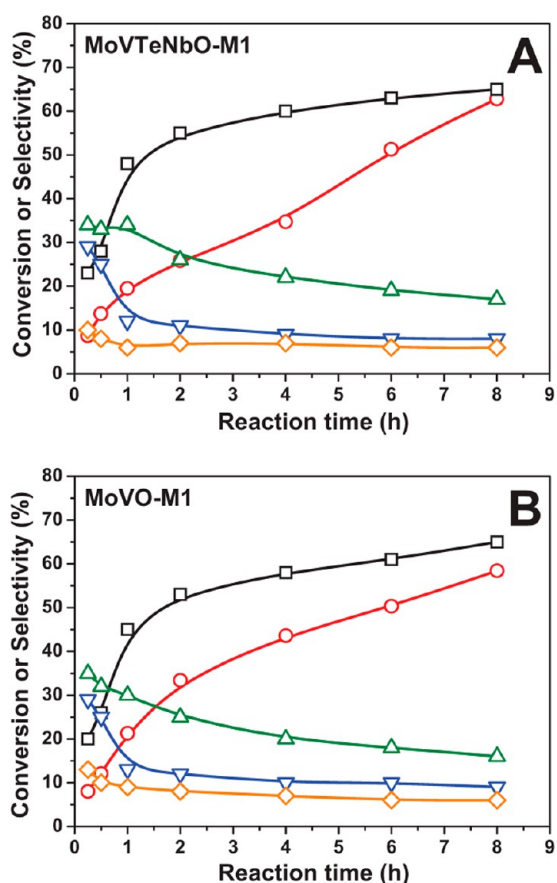
Figure 7. Catalytic performance in benzyl alcohol oxidation: conversion of benzyl alcohol (A) and product distribution (B). Reaction conditions: 10 g of benzyl alcohol, solventless, 0.5 g of catalyst, T = 393 K, p_{O2} = 2 atm, reaction time of 8 h. **I-a** was also tested in inert N_2 atmosphere instead of O_2.

Figure 8. Conversion of benzyl alcohol (black squares), as well as selectivity toward benzaldehyde (red circles), benzoic acid (green triangles), benzyl benzoate (blue triangles), and toluene (orange diamonds) in benzyl alcohol oxidation as a function of reaction time for the catalysts **I-a** (A) and **III** (B). Reaction conditions: 5 g of benzyl alcohol, 0.25 g of catalyst, T = 393 K, p_{O2} = 2 atm.

reaction media, excluding possible involvement of in situ generated hydrogen peroxide in the oxidation reaction. No significant change is detected by the XRD, IR and SEM measurements of the spent **I-a** (not shown), indicating that the M1 structure is preserved in the course of the catalytic reaction.

3.3.1. Comparison of MoV and MoVTeNb M1 Oxides. Interestingly, the quinary MoVTeNb M1 oxide **I-a** and **I-b** and the ternary MoV M1 oxide **III** showed quite similar performances with respect to the activity (Figure 7A), the selectivity (Figure 7B), and the time evolution of the reaction (Figure 8). Obviously, the elemental composition of the M1 compounds shows no influence, which is in contrast to the propane oxidation. The active sites probably consist of Mo−V−O[31] or V−O−V motifs, and the presence of Nb and Te is not necessary for the reaction.

Significant difference in the activity was found within the phase-pure quinary MoVTeNb M1 oxide. While **I-a** and **I-b** showed similar catalytic performance, the activity of **II** was much lower than **I-a** and **I-b** (Figure 6). This result is in contrast to the high activity and selectivity of **II** in propane oxidation (Figures 4 and 5). The low activity of **II** can be partially attributed to the low surface area (Table 1). However, intrinsically low activity of **II** is evident from the activity normalized by the surface area (Figure 5B). The different intrinsic activities are likely because of differences in the termination of the M1, which renders the nature and density of active sites different. Again, the termination strongly depends on the preparation method and results in different surface compositions. The excessive segregation of Te on the surface of

II (Table 1, Figure 6) may be the reason for blockage of active Mo−O−V or V−O−V sites.

3.3.2. Oxidation Products and Mechanistic Considerations. The reaction yielded benzaldehyde with about 70% selectivity, while benzoic acid, benzyl benzoate, and toluene are detected in minor quantities over all the M1 catalysts (Figure 7B). The formation of various oxidation products indicates multiple functions of the M1 catalysts. Scheme 2 shows a likely reaction network for the formation of the products. Modest formation of benzaldehyde, benzyl benzoate, and benzoic acid occur even in the absence of gas phase oxygen (Figure 7, **I-a** in

Scheme 2. Suggested Reaction Scheme of the Benzyl Alcohol Oxidation
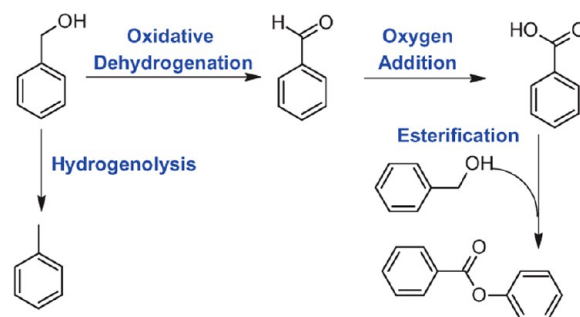
N$_2$), suggesting that the oxidation reactions proceed under these conditions by reduction of the catalysts.

3.3.2.1. Oxidative Dehydrogenation to Benzaldehyde. The formation of benzaldehyde shows the ability of the oxidative dehydrogenation of benzyl alcohol. It is likely that active sites for alcohol oxidation contain a V^{5+} center.[7,38,39] General pathways of the oxidative dehydrogenation of alcohols over metal (Mo and V) oxide catalysts have been established. The first step of catalytic oxidation of alcohols is the dissociative adsorption of the hydroxyl group of the alcohol, which yields a surface alkoxide group coordinated to the metal atom and a hydroxyl group. This can happen either by cleavage of a metal−oxygen−metal bridge (Scheme 3a) or without breaking the

Scheme 3. Suggested Mechanisms for the Oxidation of Benzyl Alcohol to Benzaldehyde: With (a) and without (b) Involving the Opening of the M−O−M Bond

M = V^{5+} or Mo^{6+}, M = V^{4+} or Mo^{5+}
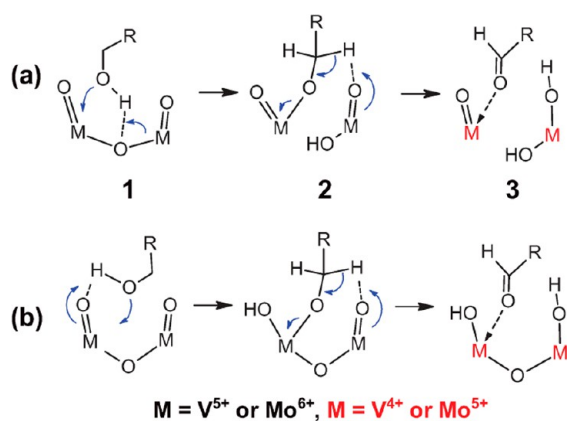
bond in case when the metal exist in a highly distorted coordination offering a coordination site for the oxygen atom of the alcohol molecule (Scheme 3b). Subsequently, the abstraction of a hydrogen takes place by the red-ox function of metal−oxygen moieties to yield the aldehyde.[40−44] In situ IR investigations have shown that the oxidative dehydrogenation of alcohols to carbonyl compounds is a facile reaction that can take place even at room temperature in the absence of molecular oxygen under reduction of the corresponding surface.[41,45] Therefore, the demands with respect to the surface oxygen species, which accept the hydrogen from the reactant alcohol, are comparatively low in contrast to the abstraction of a hydrogen atom from a C−H bond in the oxidative dehydrogenation of alkane molecules. In the latter case, strongly polarized metal oxo oxygen atoms (M=O) are probably preferred rather than bridging oxygen atoms (M−O−M).[35]

Taking into account these considerations, we suggest a possible reaction mechanism in Scheme 3. We assume here arbitrary a dimetal site containing M−O−M bridges (M = Mo, V). The first step is the formation of a metal alkoxide and a hydroxyl group (Scheme 3, 1 to 2) through a concerted nucleophile−electrophile interaction. The nucleophilic vanadyl oxygen abstracts alcoholic hydrogen, while the alcoholic oxygen concurrently attacks the electron deficient (i.e., Lewis acidic) coordinatively unsaturated V^{5+} center. The second step (Scheme 3, 2 to 3) is the abstraction of the formyl hydrogen by a nucleophilic oxygen belonging to the metal in its highest oxidation state in the vicinity, involving concurrent one electron reduction of the two metal centers (i.e., total two electrons

reduction). We consider that in the required two-electron reduction the sharing of two metal centers is preferred instead of a single metal center. In this regard, the oxidative dehydrogenation of benzyl alcohol to benzaldehyde probes the abundance of di- or multimetal oxide sites on the surface of the catalyst.

3.3.2.2. Formation of Byproducts. The formation of benzoic acid indicates the presence of an additional oxidation function on the surface of the catalyst, which is capable to catalyze oxygen insertion into the aldehyde functional group. While the oxidative dehydrogenation of the alcohol to the aldehyde requires only nucleophilic oxygen, the oxygen insertion possibly involves the addition of electrophilic oxygen. Benzyl benzoate is likely formed by the condensation of benzoic acid with benzyl alcohol (Scheme 2) assisted by acid sites. The selectivity to benzoic acid or benzyl benzoate, respectively, were relatively high at the initial period of the reaction and decreased at prolonged reaction time (Figure 8), indicating the deactivation of the oxygen addition function. It appears that the oxygenation function of M1 strongly depends on the temperature. Weak oxygenation function occurs at the present reaction temperature (393 K), while little acid formation (selectivity to benzaldehyde >95%) has been reported over a similar MoV M1 oxide at 353 K.[31] Likewise, the main product of ethanol oxidation over MoVTeNb oxides changes from acetaldehyde to acetic acid upon increasing the temperature from 373 to 573 K.[30] It is speculated that the oxygenating electrophilic oxygen attacks and ruptures the electron-rich olefinic bond of intermediates and the product in the case of propane oxidation (e.g., propene, acrolein, acrylic acid) and lead to the unselective oxidation to CO$_x$ at elevated temperature.

Finally, the formation of toluene requires a hydrogenolysis function, which is speculated to be possible because of the bronze-like nature of the partially reduced suboxides leading to the hydrogenolysis of benzyl alcohol to toluene even in the presence of dissolved oxygen.

3.4. Comparison of Propane Oxidation and Benzyl Alcohol Oxidation. The surface area normalized consumption rates of benzyl alcohol are comparable or even higher compared to that of propane (Figure 5). The activation of the first C−H bond in propane is a quite demanding reaction that requires high reaction temperatures of 653−673 K or highly active oxygen species. Moreover, the two reactions show different ranking of the catalysts with respect to the consumption rates. The rate of consumption of the substrate molecule decreases in the order II > I-b > III for propane oxidation (Figure 5A), while the order I-b ≈ I-a > II ≈ III is observed for benzyl alcohol oxidation (Figure 5B). On the basis of these observations and the mechanistic considerations discussed in sections 3.2.2 and 3.3.2, we suggest that different types of active sites on M1-type oxides are involved in the activation of propane and benzyl alcohol.

Concerning the activation of the C−H bond in propane, vanadyl oxygen atoms[35] have been considered as the active sites for the radicalic activation.[3,4,35] It is likely that only a minor fraction of the surface vanadyl sites are equipped with the ability to activate stable paraffinic C−H bonds.[23] Low density of propane activating sites would account for a low consumption rate of propane despite high reaction temperature. Accordingly, adsorption sites that are not relevant for propane activation very likely coexist and these species could represent active sites for benzyl alcohol oxidation. In addition, the ODP sites might comprise a part of benzyl alcohol

oxidation sites. Owing to the presence of the alcoholic group, the activation of benzyl alcohol is a facile process and occurs via a different and much easier activation mechanism compared to that of propane. Likewise, in propane oxidation, the potential reaction intermediates (e.g., propanol, propene, allyl alcohol, and acrolein) and acrylic acid are equipped with functional groups, which can facilitate activated adsorption, which could lead to further selective and unselective oxidation. The oxidation of benzyl alcohol may, therefore, serve as a reaction, which probes the minimum requirements of an alkane oxidation catalyst.

On the basis of the observations presented in Figure 5, we speculate that the active sites in benzyl alcohol oxidation act mainly as sites for unselective oxidation (i.e., formation of CO and CO_2) under propane oxidation condition owing to the increased reactivity at elevated temperature. Ternary MoV M1 oxide catalysts show excellent activity and selectivity (>90%) in acrolein oxidation to acrylic acid at moderate temperature (463 K);[29] however, the formation of CO_x becomes predominant at temperatures required for the activation of propane (>593 K).[12] Significant increase of CO_x formation at elevated temperature has been also reported in the oxidation of allyl alcohol (which is similar to benzyl alcohol in the view of conjugated stabilization in the course of oxidation) over a ternary Mo−V−O oxide catalyst.[7] In the present benzyl alcohol oxidation, the low reaction temperature (393 K) allows to avoid extensive overoxidation of products, whereas the same sites would become sufficiently reactive to decompose C3 compounds other than propane at propane oxidation condition (653−673 K). This speculation can explain the observation that the more selective propane oxidation catalyst II (Figure 4C) shows lower activity as well as benzoic acid selectivity (i.e., indication for a weaker oxygen insertion function) than I-b (Figure 6) that is less selective in propane oxidation.

3.5. Activation of Molecular Oxygen. Remarkably, the oxygen consumption rate level is within the same range for both reactions despite the significant different reaction temperatures (Figure 5). The activation of molecular oxygen is involved in the two catalytic oxidation reactions. In propane oxidation, the activation of oxygen is not included in the rate-determining step, as has been indicated by the zero reaction order with respect to oxygen.[12,46] In the benzyl alcohol oxidation, the observed significant oxygen consumption rates suggest that oxygen activation is not limiting.

We consider that the fast completion of the reoxidation of M1 (i.e., reduction of O_2 to $2O^{2-}$) avoids the presence of electrophilic oxygen species on the surface and thus contributes to the high selectivity in propane oxidation to acrylic acid. The reduction of a dioxygen may proceed in a sequential pathway involving four electrons: $O_2 \rightarrow O_2^- \rightarrow O_2^{2-} (\rightarrow 2O^-) \rightarrow 2O^{2-}$. It is known that partially reduced oxygen species (i.e., O_2^-, O_2^{2-} and O^-) are strongly electrophilic radical reactants that lead to the degradation of the carbon skeleton forming CO_x.[47−49] Fast kinetics of the reduction of molecular oxygen by the reduced M1 surface avoids the presence of these oxygen species. We have found negligible activity of M1 in CO oxidation that requires electrophilic oxygen,[50] indicating the absence of partially reduced O_2. Selective partial oxidation catalysts are often characterized by very weak dependence on oxygen partial pressure.[12,39−41]

3.6. Functional Sites in Alkane and Alcohol Oxidation. Taking into account all the experimental results, we discuss the different requirements in alcohol and alkane oxidation on the surface of molybdenum−vanadium-based mixed oxide catalysts in Scheme 4. The surface of the catalysts is dynamically

Scheme 4. Illustration of the Functional Model of MoV(TeNb) M1 Oxides in Oxidation of Propane and Benzyl Alcohol
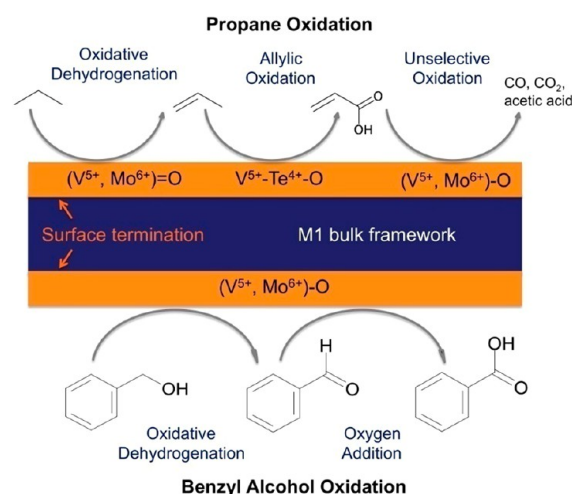
reconstructed under reaction conditions as evidenced by in situ photoelectron spectroscopy.[22,23] In propane oxidation at elevated temperature (e.g., 653 K) it is assumed that vanadyl oxygen performs the ODP to propene by a radical mechanism on supported vanadium oxide.[35] Terminal oxygen atoms may also be responsible for propane activation on M1. Subsequently, readsorbed propene may undergo selective oxidation to acrylic acid over $M^{n+}−O−M^{n+}$ ensemble sites that contain V^{5+} and probably Te^{4+}.[23] Alternatively, acrolein may desorb from these sites and rapidly be oxidized to acrylic acid on Mo−O−V sites.[12,25] The formation of the $V^{5+}−O−Te^{4+}$ ensemble sites partially blocks V(Mo)−O−V sites that are responsible for the CO_x formation, leading to a high selectivity to acrylic acid. Since considerable accumulation of $V^{5+}−O−Te^{4+}$ ensemble sites on the surface of MoVTeNb M1 oxide was only observed under conditions at which predominantly acrylic acid was observed in the gas phase, but no propene (in presence of steam in the feed),[23] it would be also possible that the nature of the active sites and consequently the reaction mechanism changes by changing the reaction conditions resulting in a mechanism that involves other pathways.

In the low temperature (393 K) benzyl alcohol oxidation, oxidative dehydrogenation of the alcohol to the aldehyde takes place on the Mo−V−O matrix by a nonradicalic bifunctional mechanism involving cooperation of acid−base and redox functions, which is in contrast to the assumed radical activation of propane at elevated temperature. The oxygen addition function operates moderately at 393 K, yielding benzoic acid (and benzyl benzoate) in minor quantities.

The direct comparison of propane oxidation and benzyl alcohol oxidation on the same mixed oxides revealed that at temperatures required for propane oxidation, the oxygenation functions of a catalyst that selectively insert oxygen at low temperature lead to unselective oxidation to CO_x. This may be, in the end, also attributed to the surface dynamics of the catalysts under investigation. Currently, extensive surface characterization of the catalysts under operation is under way. The fast kinetics of the reoxidation of reduced M1 is another

prominent property of the M1-type oxides, which we consider relevant to the selectivity to partial oxidation products, and which is not described in Scheme 4.

4. CONCLUSIONS

We investigated the reactivity of mixed MoV(TeNb) oxides composed of the orthorhombic M1 structure beyond propane oxidation to shed light on catalytic functions that are hidden under the harsh propane oxidation conditions. The striking finding is that the reaction rates of benzyl alcohol oxidation are as high as propane oxidation despite the enormous difference in the reaction temperature. This observation indicates a high ability of M1 in oxidative dehydrogenation, as well as of dioxygen activation. Assuming the independence of the reduction and reoxidation events in the catalytic cycles, rapid dioxygen activation may contribute to the high selectivity of M1 in propane oxidation.

The analysis of the reactivity data suggests the presence of several types of active sites on the M1 surface. Depending on the type of the reacting organic molecule, different modes of adsorption, thus oxidation mechanisms, take place. The densities of the various types of active sites are variable even within highly crystalline MoVTeNb M1 oxide catalysts, suggesting the importance of surface termination and site occupation statistic of the M1 structure. The general view that the surface of selective oxidation catalysts differs structurally and chemically from the bulk crystal structure, which has been observed in case of different systems including phosphates and mixed oxides,[22,23,51] is increasingly accepted in mechanistic and structural considerations of selective oxidation reactions.[52] Acrylic acid formation in propane oxidation owes to the incorporation of Te and Nb in the M1 framework. The decoration of the M1 surface with V^{5+} and Te^{4+} induced under propane oxidation conditions may be responsible for oxidation of the intermediate propene to acrylic acid. The benzyl alcohol oxidation was insensitive to the presence of Te and Nb, implying the catalytic function for the acrylic acid formation does not exist or does not operate at the mild reaction condition of alcohol oxidation.

The direct transformation of propane to acrylic acid involves various surface intermediates having different reactivity. The diversity of sites present on the surface of the complex MoVTeNb oxide contributes to the appearance of a complicated reaction network when intermediates desorb from these sites. The present comparison of two reactants having significantly different reactivity reveals the presence of multiple catalytic functions on the surface of the M1 phase, highlighting the underlying complexity of the surface and catalysis of the M1 structure. We still lack a picture of the whole interplay and identification of multiple active sites existing on the surface of the working M1 phase. An extended and systematic reactivity study in conjunction with surface characterization is the subject of current research.

■ ASSOCIATED CONTENT

ⓢ Supporting Information

Rietveld analysis of the XRD patters. This material is available free of charge via the Internet at http://pubs.acs.org

■ AUTHOR INFORMATION

Corresponding Author

*E-mail: trunschke@fhi-berlin.mpg.de.

Present Address

‡International Iberian Nanotechnology Laboratory, Av. Mestre José Veiga, s/n, P-4715-330 Braga, Portugal.

Notes

The authors declare no competing financial interest.

■ ACKNOWLEDGMENTS

■ REFERENCES

(1) Ushikubo, T.; Sawaki, I.; Oshima, K.; Inumaru, K.; Kobayakawa, S.; Kiyono, K. Process for preparing a catalyst useful for producing a nitrile. United States Patent US5422328, June 6, 1995.

(2) Trunschke, A. In *RSC Nanoscience & Nanotechnology*; Hess, C., Schlögl, R., Eds.; Royal Society of Chemistry: Cambridge, 2011; pp 56−95.

(3) Grasselli, R.; Buttrey, D.; DeSanto, P.; Burrington, J.; Lugmair, C.; Volpe, A.; Weingand, T. *Catal. Today* **2004**, *91−92*, 251−258.

(4) Schlögl, R. *Top. Catal.* **2011**, *54*, 627−638.

(5) DeSanto, P.; Buttrey, D.; Grasselli, R.; Lugmair, C.; Volpe, A.; Toby, B.; Vogt, T. *Z. Kristallogr.* **2004**, *219*, 152−165.

(6) Oshihara, K.; Hisano, T.; Ueda, W. *Top. Catal.* **2001**, *15*, 153−160.

(7) Guliants, V. V.; Bhandari, R.; Hughett, A. R.; Bhatt, S.; Schuler, B. D.; Brongersma, H. H.; Knoester, A.; Gaffney, A. M.; Han, S. *J. Phys. Chem. B* **2006**, *110*, 6129−6140.

(8) Ivars, F.; Solsona, B.; Hernández, S.; López Nieto, J. M. *Catal. Today* **2010**, *149*, 260−266.

(9) Baca, M.; Pigamo, A.; Dubois, J. L.; Millet, J. M. M. *Top. Catal.* **2003**, *23*, 39−46.

(10) Holmberg, J.; Grasselli, R. K.; Andersson, A. *Appl. Catal., A* **2004**, *270*, 121−134.

(11) Naraschewski, F. N.; Jentys, A.; Lercher, J. A. *Top. Catal.* **2011**, *54*, 639−649.

(12) Ueda, W.; Vitry, D.; Katou, T. *Catal. Today* **2005**, *99*, 43−49.

(13) Guliants, V. V.; Bhandari, R.; Swaminathan, B.; Vasudevan, V. K.; Brongersma, H. H.; Knoester, A.; Gaffney, A. M.; Han, S. *J. Phys. Chem. B* **2005**, *109*, 24046−24055.

(14) Pyrz, W.; Blom, D.; Shiju, N.; Guliants, V.; Vogt, T.; Buttrey, D. *J. Phys. Chem. C* **2008**, *112*, 10043−10049.

(15) Li, X.; Buttrey, D. J.; Blom, D. A.; Vogt, T. *Top. Catal.* **2011**, *54*, 614−626.

(16) Blom, D. A.; Li, X.; Mitra, S.; Vogt, T.; Buttrey, D. J. *ChemCatChem* **2011**, *3*, 1028−1033.

(17) Callahan, J. L.; Grasselli, R. K. *AIChE J.* **1963**, *9*, 755−760.

(18) Grasselli, R. *Catal. Today* **2005**, *99*, 23−31.

(19) Celaya Sanfiz, A.; Hansen, T. W.; Sakthivel, A.; Trunschke, A.; Schlögl, R.; Knoester, A.; Brongersma, H. H.; Looi, M. H.; Hamid, S. B. A. *J. Catal.* **2008**, *258*, 35−43.

(20) Shiju, N. R.; Liang, X.; Weimer, A. W.; Liang, C.; Dai, S.; Guliants, V. V. *J. Am. Chem. Soc.* **2008**, *130*, 5850−5851.

(21) Guliants, V. V.; Bhandari, R.; Brongersma, H. H.; Knoester, A.; Gaffney, A. M.; Han, S. *J. Phys. Chem. B* **2005**, *109*, 10234−10242.

(22) Celaya Sanfiz, A.; Hansen, T. W.; Teschner, D.; Schnörch, P.; Girgsdies, F.; Trunschke, A.; Schlögl, R.; Looi, M. H.; Hamid, S. B. A. *J. Phys. Chem. C* **2010**, *114*, 1912−1921.

(23) Hävecker, M.; Wrabetz, S.; Kröhnert, J.; Csepei, L.-I.; Naumann d'Alnoncourt, R.; Kolen'ko, Y. V.; Girgsdies, F.; Schlögl, R.; Trunschke, A. *J. Catal.* **2012**, *285*, 48−60.

(24) Balcells, E.; Borgmeier, F.; Grißtede, I.; Lintz, H.-G. *Catal. Lett.* **2003**, *87*, 195−199.

(25) López Nieto, J. M.; Solsona, B.; Concepción, P.; Ivars, F.; Dejoz, A.; Vázquez, M. I. *Catal. Today* **2010**, *157*, 291−296.

(26) Naumann d'Alnoncourt, R.; V. Kolen'ko, Y.; Schlogl, R.; Trunschke, A. *Comb. Chem. High Throughput Screening* **2012**, *15*, 161−169.

(27) Kolen'ko, Y. V.; Zhang, W.; d' Alnoncourt, R. N.; Girgsdies, F.; Hansen, T. W.; Wolfram, T.; Schlögl, R.; Trunschke, A. *ChemCatChem* **2011**, *3*, 1597−1606.

(28) Luo, L.; Labinger, J. A.; Davis, M. E. *J. Catal.* **2001**, *200*, 222−231.

(29) Sadakane, M.; Watanabe, N.; Katou, T.; Nodasaka, Y.; Ueda, W. *Angew. Chem., Int. Ed.* **2007**, *46*, 1493−1496.

(30) Sobolev, V. I.; Koltunov, K. Y. *ChemCatChem* **2011**, *3*, 1143−1145.

(31) Wang, F.; Ueda, W. *Appl. Catal., A* **2008**, *346*, 155−163.

(32) Wang, F.; Ueda, W. *Top. Catal.* **2008**, *50*, 90−97.

(33) Wang, F.; Ueda, W. *Catal. Today* **2009**, *144*, 358−361.

(34) Watanabe, N.; Ueda, W. *Ind. Eng. Chem. Res.* **2006**, *45*, 607−614.

(35) Rozanska, X.; Fortrie, R.; Sauer, J. *J. Phys. Chem. C* **2007**, *111*, 6041−6050.

(36) Kolen'ko, Y. V.; Amakawa, K.; Naumann d'Alnoncourt, R.; Girgsdies, F.; Weinberg, G.; Schlögl, R.; Trunschke, A. *ChemCatChem* **2012**, *4*, 495−503.

(37) Grasselli, R. K.; Lugmair, C. G.; Volpe, A. F. *Top. Catal.* **2011**, *54*, 595−604.

(38) Wachs, I. E.; Jehng, J.-M.; Ueda, W. *J. Phys. Chem. B* **2005**, *109*, 2275−2284.

(39) Tang, Q.; Chen, Y.; Yang, Y. *J. Mol. Catal. A: Chem.* **2010**, *315*, 43−50.

(40) Banares, M. A.; Hu, H. C.; Wachs, I. E. *J. Catal.* **1994**, *150*, 407−420.

(41) Busca, G. *Langmuir* **1986**, *2*, 577−582.

(42) Gregoriades, L. J.; Döbler, J.; Sauer, J. *J. Phys. Chem. C* **2010**, *114*, 2967−2979.

(43) Burcham, L. J.; Briand, L. E.; Wachs, I. E. *Langmuir* **2001**, *17*, 6175−6184.

(44) Nair, H.; Gatt, J. E.; Miller, J. T.; Baertsch, C. D. *J. Catal.* **2011**, *279*, 144−154.

(45) Davydov, A. *Molecular Spectroscopy of Oxide Catalyst Surface*; John Wiley & Sons Ltd.: Chichester, U.K., 2003.

(46) Balcells, E.; Borgmeier, F.; Grißtede, I.; Lintz, H.-G.; Rosowski, F. *Appl. Catal., A* **2004**, *266*, 211−221.

(47) Grzybowska-Świerkosz, B. *Top. Catal* **2000**, *11−12*, 23−42.

(48) Haber, J. In *Handbook of Heterogeneous Catalysis*; Ertl, G., Knözinger, H., Schüth, F., Weitkamp, J., Eds.; Wiley-VCH Verlag GmbH & Co. KGaA: Weinheim, Germany, 2008; pp 3359−3384.

(49) Rozanska, X.; Kondratenko, E. V.; Sauer, J. *J. Catal.* **2008**, *256*, 84−94.

(50) Freund, H.; Meijer, G.; Scheffler, M.; Schlögl, R.; Wolf, M. *Angew. Chem., Int. Ed.* **2011**, *50*, 10064−10094.

(51) Hävecker, M.; Mayer, R. W.; Knop-Gericke, A.; Bluhm, H.; Kleimenov, E.; Liskowski, A.; Su, D.; Follath, R.; Requejo, F. G.; Ogletree, D. F.; Salmeron, M.; Lopez-Sanchez, J. A.; Bartley, J. K.; Hutchings, G. J.; Schlögl, R. *J. Phys. Chem. B* **2003**, *107*, 4587−4596.

(52) Wachs, I. E.; Routray, K. *ACS Catal.* **2012**, *2*, 1235.